Available online at www.sciencedirect.com
SCIENCE DIRECT®
Journal of Solid State Chemistry 177 (2004) 979–986
JOURNAL OF SOLID STATE CHEMISTRY
http://elsevier.com/locate/jssc

An electron diffraction and bond valence sum study of the space group symmetries and structures of the photocatalytic 1:1 ordered A_2InNbO_6 double perovskites ($A = Ca^{2+}$, Sr^{2+}, Ba^{2+})

V. Ting, Y. Liu, R.L. Withers,* and E. Krausz

Research School of Chemistry, Australian National University, Science Road, Canberra ACT 0200, Australia

Received 29 August 2003; accepted 29 September 2003

Abstract

A careful investigation has been carried out into the space group symmetries, structures and crystal chemistries of the 1:1 *B*-site ordered double perovskites A_2InNbO_6 ($A = Ca^{2+}$, Sr^{2+}, Ba^{2+}) using a combination of bond valence sum calculations, powder XRD and electron diffraction. A recent investigation of these compounds by Yin et al. reported a random distribution of In^{3+} and Nb^{5+} ions onto the perovskite *B*-site positions of these compounds and hence $Pm\bar{3}m$ ($a = a_p$, subscript p for parent perovskite sub-structure) space group symmetry for the A = Ba and Sr compounds and *Pnma* ($\mathbf{a} = \mathbf{a}_p + \mathbf{b}_p$, $\mathbf{b} = -\mathbf{a}_p + \mathbf{b}_p$, $\mathbf{c} = 2\mathbf{c}_p$) space group symmetry for the A = Ca compound. A careful electron diffraction study, however, shows that both the A = Ca and Sr compounds occur at room temperature in $P12_1/n1$ ($\mathbf{a} = \mathbf{a}_p + \mathbf{b}_p$, $\mathbf{b} = -\mathbf{a}_p + \mathbf{b}_p$, $\mathbf{c} = 2\mathbf{c}_p$) perovskite-related superstructure phases while the A = Ba compound occurs in the $Fm\bar{3}m$, $a = 2a_p$, elpasolite structure type. Bond valence sum calculations are used to explain why this should be so as well as to provide a useful first-order approximation to the structures of each of the compounds.
© 2003 Elsevier Inc. All rights reserved.

Keywords: Electron diffraction; Bond valence; Double perovskites

1. Introduction

ABO_3 perovskites, along with numerous *A* and *B* sites substituted $A_{1-x}A'_xB_{1-y}B'_yO_{3-\delta}$ variants thereof, have long been studied as a result of their inherent displacive flexibility [1–3], subtle polymorphic phase transition behavior as a function of temperature and/or composition [3–6] and potential technological applications, e.g. as fast oxide ion conductors in solid oxide fuel cells [7], as microwave-range dielectric resonators [8,9], etc. Recently, $A(In_{0.5}Nb_{0.5})O_3$ (A = Ba, Sr and Ca) perovskites have been the subject of investigation [10] due to their potential application as visible light-driven semiconductor photocatalysts for the evolution of H_2 from water for hydrogen fuel cells.

Yin et al. [10] described the In^{3+} and Nb^{5+} ions on the perovskite *B*-sites of these compounds as being distributed "…randomly in a charge balanced manner …", i.e. they reported random *B*-site ordering rather than the more common rock salt type ordering [5]. The $Ba(In_{0.5}Nb_{0.5})O_3$ and $Sr(In_{0.5}Nb_{0.5})O_3$ compounds were thus reported to be metrically cubic and of $Pm\bar{3}m$ space group symmetry ($a = a_p = 4.1454$ and 4.0569 Å, respectively, subscript p for the underlying perovskite parent sub-structure) while the metrically orthorhombic $Ca(In_{0.5}Nb_{0.5})O_3$ compound was reported as having space group symmetry *Pnma*, $a \sim \sqrt{2}a_p = 5.532$, $b \sim \sqrt{2}a_p = 5.715$ and $c \sim 2a_p = 7.918$ Å.

While *B*-site ordering is most often found in $A_2BB'O_6$ compounds, random *B*-site ordering is also reasonably common, particularly when the charge difference between the *B* and *B'* ions is $\leqslant 2$ (see Table 1 of Ref. [5]). Additional support for random *B*-site ordering is provided by a recent Raman study of *B*-site ordering in $Sr(B_{0.5}Nb_{0.5})O_3$ compounds [11]. The authors reported a "…remarkable change in the Raman spectrum of the In compound…" by comparison with most of the other compounds investigated with "…most of the spectral features…unresolved…". The observed behavior was

*Corresponding author. Fax: +61-02-61250750.
E-mail address: withers@rsc.anu.edu.au (R.L. Withers).

0022-4596/$ - see front matter © 2003 Elsevier Inc. All rights reserved.
doi:10.1016/j.jssc.2003.09.040

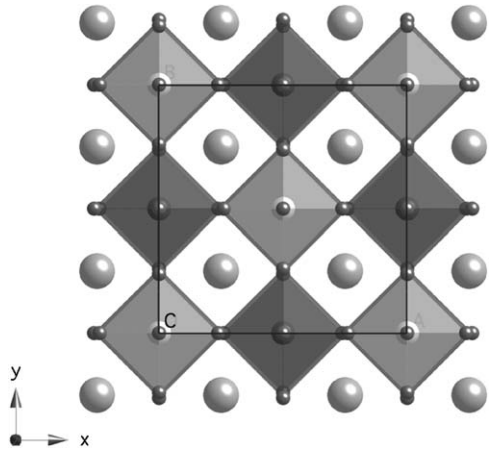

Fig. 1. Shows the ideal rock salt ordering and associated expansion/contraction of the local BO_6 and $B'O_6$ octahedra characteristic of the $Fm\bar{3}m$, $a = 2a_p$ double perovskite (or elpasolite) structure type in projection down an [001] direction. The larger BO_6 octahedra are represented by the darker octahedra while the lighter octahedra represent the smaller $B'O_6$ octahedra. The A ions are presented by the largest balls and the O ions by the smallest balls.

reported to be similar to that observed in B-site disordered $Pb(In_{0.5}Nb_{0.5})O_3$ and attributed to "... disorder in the B-ion sublattice..." [11].

On the other hand, early X-ray powder diffraction (XRPD) structural investigations of $BaIn_{0.5}Nb_{0.5}O_3$ [12] and $SrIn_{0.5}Nb_{0.5}O_3$ [13] reported weak additional superstructure lines indicative of B-site cation ordering and doubled $a = 2a_p$ (=8.279 and 8.106 Å, respectively), metrically cubic unit cells. No space group symmetries were, however, suggested in either case. (Note that rock salt ordering and associated expansion/contraction of the local BO_6 and $B'O_6$ octahedra (see Fig. 1) formally gives rise to an $Fm\bar{3}m$, $a = 2a_p$ structure [5,6].) Likewise, Filip'ev and Fesenko [14] reported In^{3+}/Nb^{5+} ordering for the $SrIn_{0.5}Nb_{0.5}O_3$ [14] compound and essentially the same metrically orthorhombic cell as given by Yin et al. [10]. Again, however, no space group symmetry was given.

In light of these ambiguities and the known sensitivity of electron diffraction to weak features of reciprocal space, a detailed electron diffraction and bond valence sum study of the unit cells and space group symmetries of the photocatalytic A_2InNbO_6 double perovskites has therefore been carried out.

2. Experimental

Stoichiometric ratios of $BaCO_3$ (4 N, Aldrich), $SrCO_3$ (5 N, Alfa) or $CaCO_3$ (5 N, Alfa) were mixed together with In_2O_3 (4 N, Aldrich) and Nb_2O_5 (>3 N, Alfa) and ground to an intimate powder under ethanol in an agate mortar. The resultant powder was first thermally treated in an 850°C furnace for a 20 h period to drive off CO_2, then pressed into pastilles and calcined at 1230°C for a period of 48 h. In the case of the A = Ba and Ca compounds, the $AIn_{0.5}Nb_{0.5}O_3$ samples thereby obtained were single phase. In the case of the A = Sr compound, the initially obtained sample was two-phase, consisting of a minority metastable phase and the true equilibrium phase. Upon re-grinding and further thermal annealing of 2–4 days, the metastable phase disappeared leaving the single phase equilibrium product.

Powder samples of the fired pastilles were analyzed via XRPD using a Guinier–Hägg XRD camera with a Cu$K\alpha$1 radiation source. Silicon (NBS No. 640) was added as an internal standard for accurate determination of the unit cell dimensions, refined using the Unitcell software package.

Transmission electron microscope (TEM) analysis was carried out in a Philips EM 430 TEM on crushed grains of the samples dispersed on holey carbon coated copper grids.

The Raman spectrum was collected using the 488 nm line (300 mW) of a Spectra Physics model 164 Argonion laser in conjunction with a Spex 1401 double monochromator operating at 3 cm^{-1} resolution. The photocurrent from a Hamamatsu R-943-02 photomultiplier tube was passed through a Stanford Research SR445 pulse amplifier to a Stanford Research SR400 photon counter. The spectrometer was interfaced with a PC.

3. Results and discussion

3.1. X-ray powder diffraction

The Guinier pattern of $BaIn_{0.5}Nb_{0.5}O_3$ showed a metrically cubic parent perovskite unit cell with $a = 4.1427(4)$ Å in good agreement with Yin et al. [10]. Neither split parent perovskite lines nor additional superlattice lines were detectable.

The Guinier pattern of the equilibrium $SrIn_{0.5}Nb_{0.5}O_3$ compound again showed a metrically cubic parent perovskite unit cell with $a_p = 4.0547(2)$ Å with no evidence for line splitting even at quite high angle. This time, however, weak additional superlattice lines were clearly visible. All lines could be successfully indexed either to an $a = 2a_p = 8.1094(4)$ Å cubic unit cell or, equally well, to a tetragonal (but very close to metrically cubic) $a = 5.7357(6)$ ($=4.0557\sqrt{2}$), $b = 5.7357(6)$ ($=4.0557\sqrt{2}$) and $c = 8.1030(15)$ ($=4.0515 \times 2$ Å) unit cell. It is worth pointing out that similar weak additional superlattice lines are in fact also visible in Yin et al.'s published XRD patterns of $SrIn_{0.5}Nb_{0.5}O_3$ and $CaIn_{0.5}Nb_{0.5}O_3$ (see Fig. 1 of Ref. [10]). In that paper [10], however, these weak additional lines were attrib-

uted to an impurity phase rather than to a superstructure.

XRD analysis of the initially obtained two-phase sample showed that the minority metastable $SrIn_{0.5}Nb_{0.5}O_3$ compound was also characterized by a metrically cubic parent perovskite unit cell, but with $a_p = 4.097(7)$ Å. The corresponding diffraction lines, in this case, were somewhat broad.

In the case of the $CaIn_{0.5}Nb_{0.5}O_3$ compound, the Guinier patterns showed clear metrically orthorhombic splitting of the parent perovskite lines as well as additional weak superstructure lines. The refined, metrically orthorhombic unit-cell dimensions were $a = 5.5284(8), b = 5.7109(10)$ and $c = 7.9290(17)$ Å.

3.2. Electron diffraction

3.2.1. $Ba(In_{0.5}Nb_{0.5})O_3$

Fig. 2 shows typical (a) $\langle 001 \rangle$, (b) $\langle 111 \rangle$ and (c) $\langle 110 \rangle$ zone axis electron diffraction patterns (EDPs) of $BaIn_{0.5}Nb_{0.5}O_3$ indexed both with respect to the perovskite parent unit cell (subscript p) and a doubled superlattice unit cell with cell dimensions $2a_p \times 2b_p \times 2c_p$ (without the subscript p). When indexed with respect to such a supercell, the observed extinction conditions necessitate an F-centered Bravais lattice.

Weak $\mathbf{G} \pm \frac{1}{2} \langle 111 \rangle_p^*$ satellite reflections are clearly present (see, e.g. Fig. 2c) in agreement with [12]. The presence of such satellite reflections is certainly consistent with $Fm\bar{3}m$, rock salt type In/Nb ordering and associated pure octahedral expansion/contraction (see Fig. 1). It is at least formally, however, also compatible with rigid body octahedral rotation around either $\langle 001 \rangle_p$, $\langle 011 \rangle_p$ or $\langle 111 \rangle_p$. Correlated octahedral rotations of this sort give rise to resultant tetragonal $I4/m$, monoclinic $C2/m$ or rhombohedral $R\bar{3}$ space group symmetries (see, for example, Fig. 1 of Howard et al. [6]). In these latter cases, the lowering of rotational symmetry could be expected to give rise to a lowering of the cubic metric symmetry and extensive orientational twinning. Given the refined cubic metric symmetry, the complete absence of any evidence for orientational twinning (as judged by careful positioning of the electron probe in microdiffraction mode) and the $m\bar{3}m$ Laue symmetry of reciprocal space, the only possible resultant space group symmetry is $Fm\bar{3}m$.

3.2.2. $Ca(In_{0.5}Nb_{0.5})O_3$

Fig. 3 shows single domain (a) [100], (b) [110], (c) [010] and (d) [001] zone axis EDPs of $CaIn_{0.5}Nb_{0.5}O_3$ indexed both with respect to the perovskite parent unit cell (subscript p) and the true $\mathbf{a} = \mathbf{a}_p + \mathbf{b}_p$, $\mathbf{b} = -\mathbf{a}_p + \mathbf{b}_p$, $\mathbf{c} = 2\mathbf{c}_p$ ($\mathbf{a}^* = \frac{1}{2}[110]_p^*$, $\mathbf{b}^* = \frac{1}{2}[\bar{1}10]_p^*$, $\mathbf{c}^* = \frac{1}{2}[001]_p^*$) superstructure unit cell. (Given such a supercell, rotational twinning is only to be expected and was indeed found. For the A = Ca compound, by contrast with the A = Sr compound (see below), the size of a single domain region was quite large making it a relatively simple matter to obtain single domain EDPs. This relatively large single domain size is presumably a consequence of the significant orthorhombic metric distortion of the underlying perovskite parent sub-structure in the case of the A = Ca compound.)

When indexed with respect to the resultant supercell, the observed extinction conditions, i.e. $F(hkl)$: no condition, $F(0kl)$: no condition, $F(h0l) = 0$ unless $h + l$ is even, $F(hk0)$: no condition, $F(0k0) = 0$ unless k is even (see the characteristic Gjønnes–Moodie, or so called G–M, dark bars running through the $0\,k\,0$, k odd as well as the $h\,0\,0$, h odd convergent beam discs in Fig. 3d), necessitate a resultant monoclinic $P12_1/n1$ (standard setting $P2_1/c(6)$) space group symmetry (see Table 3.2 of Vol. A of The International Tables for Crystallography [15]) despite the orthorhombic metric symmetry. (Note that there is no orthorhombic space group symmetry compatible with all of the above-observed characteristic extinction conditions.)

Such a resultant supercell and space group symmetry is commonly observed for rotationally distorted, B-site ordered double perovskites [5]. It corresponds in the octahedral rotation notation of Glazer [1] to an $a^-a^-c^+$ rotation pattern, i.e. octahedral rotation around both the resultant **b**- and **c**-axis.

3.2.3. $Sr(In_{0.5}Nb_{0.5})O_3$

The $Sr(In_{0.5}Nb_{0.5})O_3$ compound has been left to last as a result of difficulties associated with endemic rotational micro-twinning (in the case of the equilibrium

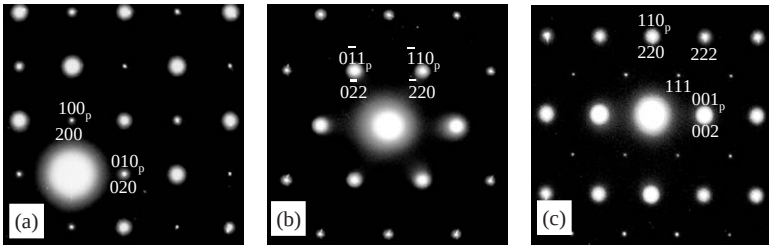

Fig. 2. (a) $\langle 001 \rangle$, (b) $\langle 111 \rangle$ and (c) $\langle 110 \rangle$ zone axis EDPs of Ba_2InNbO_6 indexed both with respect to the perovskite parent unit cell (subscript p) and a doubled superlattice unit cell with cell dimensions $2a_p \times 2b_p \times 2c_p$ (without the subscript p).

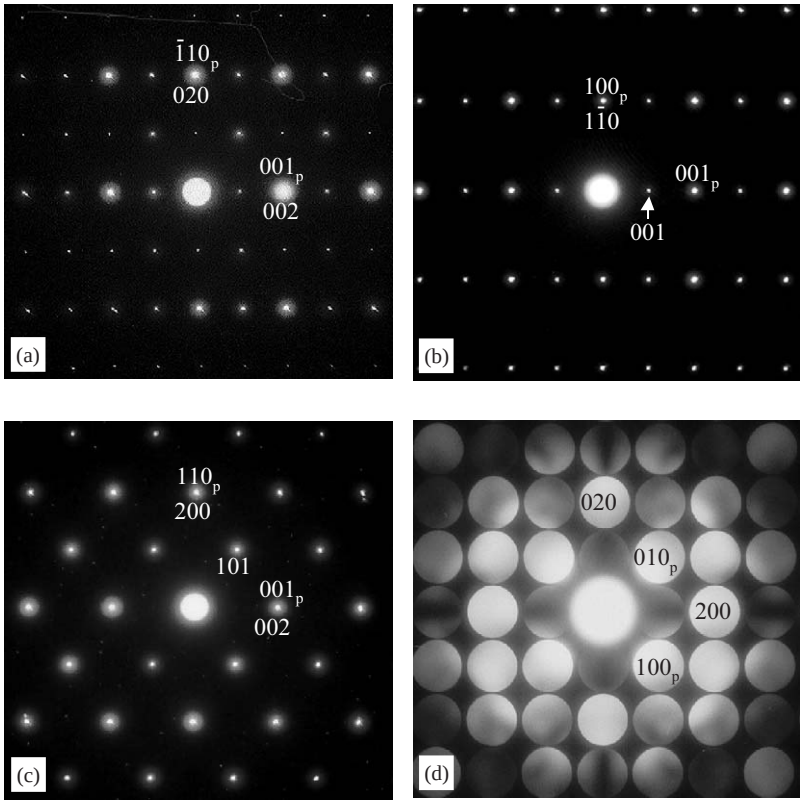

Fig. 3. Single domain (a) [100], (b) [110], (c) [010] and (d) [001] zone axis EDPs of Ca_2InNbO_6 indexed both with respect to the perovskite parent unit cell (subscript p) and the true $\mathbf{a} = \mathbf{a}_p + \mathbf{b}_p$, $\mathbf{b} = -\mathbf{a}_p + \mathbf{b}_p$, $\mathbf{c} = 2\mathbf{c}_p$ ($\mathbf{a}^* = \frac{1}{2}[110]^*_p$, $\mathbf{b}^* = \frac{1}{2}[\bar{1}10]^*_p$, $\mathbf{c}^* = \frac{1}{2}[001]^*_p$) superstructure unit cell.

compound) on an often quite fine scale (presumably a consequence of the underlying cubic metric symmetry of the perovskite parent sub-structure) as well as the existence of an additional metastable form. In spite of these difficulties, it was possible with patience, careful positioning of the electron probe and microdiffraction (when necessary) to obtain single domain (a) [100], (b) [110], (c) [010] and (d) [001] zone axis EDPs of the equilibrium $Sr(In_{0.5}Nb_{0.5})O_3$ compound (indexed again with respect to both the perovskite parent unit cell (subscript p) and the true $\mathbf{a} = \mathbf{a}_p + \mathbf{b}_p$, $\mathbf{b} = -\mathbf{a}_p + \mathbf{b}_p$, $\mathbf{c} = 2\mathbf{c}_p$ superstructure unit cell in Fig. 4).

The existence of an *n* glide perpendicular to **b** (see Fig. 4c) is again apparent as is the *P*-centered Bravais lattice and the absence of any glide extinction condition at either the [100] (see Fig. 4a) or [001] (see Fig. 4d) zone axis orientations. Given these conditions in conjunction with the recent group–subgroup analysis of Howard et al. for ordered double perovskites [6], the only possible resultant space group symmetries are either tetragonal $P4/mnc(a^0a^0c^+)$ or monoclinic $P12_1/n1(a^-a^-c^+)$. The possibility of a tertiary *c* glide perpendicular to $\langle 110 \rangle$ in the case of $P4/mnc$ can be ruled out, however, because of the presence of *h h l*, *l* odd reflections in Fig. 4b. The only possible resultant space symmetry is thus again $P12_1/n1$, just as found for the $A = Ca$ compound.

From a purely formal crystallographic point of view, an orthorhombic $Pmn2_1$ resultant space group symmetry cannot be definitively ruled out (see Table 3.2 of Ref. [15]). To distinguish between orthorhombic $Pmn2_1$ and monoclinic $P12_1/n1$ would require confirmation (or otherwise) of the $F(0k0) = 0$ unless *k* is odd condition required by $P12_1/n1$ but not by $Pmn2_1$. Unfortunately, however, the obtained [001] zone axis micro-diffraction pattern (see Fig. 4d) is not of sufficient quality in the case of the $A = Sr$ compound to confirm or otherwise this particular condition. Nonetheless, from the group theoretical point of view [6], it is clear that the only possible resultant space group symmetry is again monoclinic $P12_1/n1$, the same as definitively obtained above for the $A = Ca$ compound. This is a remarkable result given the cubic metric symmetry of the $A = Sr$ compound. It confirms once again the dangers of assigning local point group symmetries from metric symmetries alone and underlines the usefulness of electron diffraction in sorting out such ambiguities [4].

Several grains of the metastable $Sr(In_{0.5}Nb_{0.5})O_3$ compound found in the initial two-phase preparation were also investigated by electron diffraction. Fig. 5

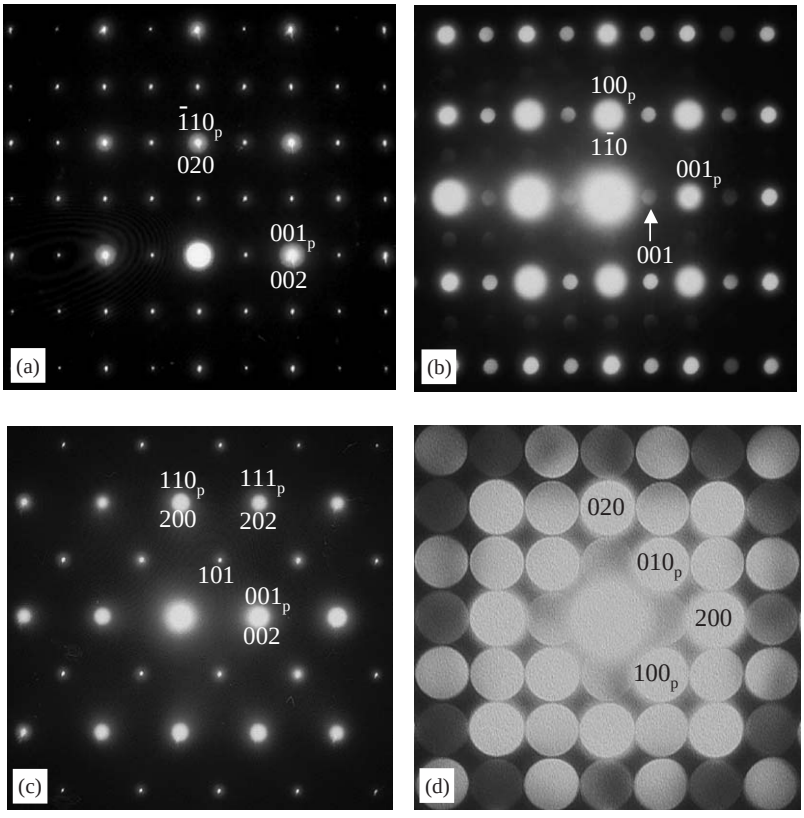

Fig. 4. Single domain (a) [100], (b) [110], (c) [010] and (d) [001] zone axis EDPs of Sr_2InNbO_6 (indexed again with respect to both the perovskite parent unit cell (subscript p) and the true $\mathbf{a} = \mathbf{a}_p + \mathbf{b}_p$, $\mathbf{b} = -\mathbf{a}_p + \mathbf{b}_p$, $\mathbf{c} = 2\mathbf{c}_p$ superstructure unit cell).

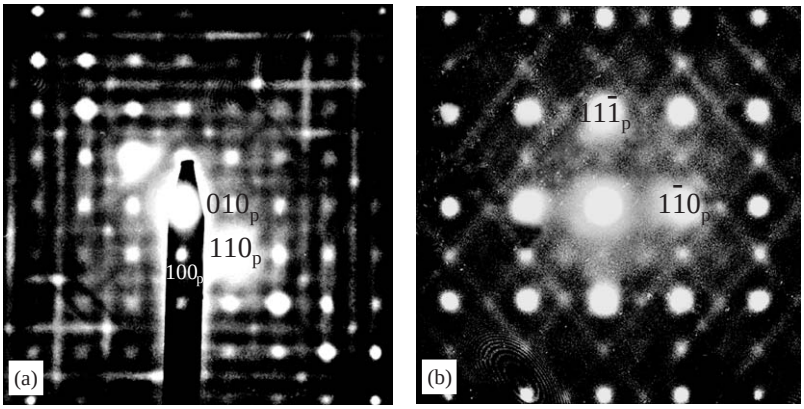

Fig. 5. Shows typical (a) close to $\langle 001 \rangle$ and (b) $\langle 112 \rangle$ zone axis EDPs of the metastable Sr_2InNbO_6 phase.

shows typical (a) close to $\langle 001 \rangle$ and (b) $\langle 112 \rangle$ zone axis EDPs of this metastable phase. No superstructure reflections in addition to the strong Bragg reflections of the underlying perovskite type average structure were detected. Note, however, the intense transverse polarized $\{hk\frac{1}{2}\}^*$ sheets of diffuse intensity perpendicular to the three $\langle 001 \rangle$ directions of the underlying average perovskite structure. Clearly, the metastable phase is *B*-site "disordered".

We believe the existence of this metastable $Sr(In_{0.5}Nb_{0.5})O_3$ compound in specimens that have not been heated for a long enough period of time provides the most likely explanation for the "unresolved… spectral features…" in the Raman spectrum of $Sr(In_{0.5}Nb_{0.5})O_3$ reported in Ref. [11] (see Fig. 4 therein). This is consistent both with the short firing time of 4 h reported in this paper as well as with the fact that the Raman spectra of the well-annealed

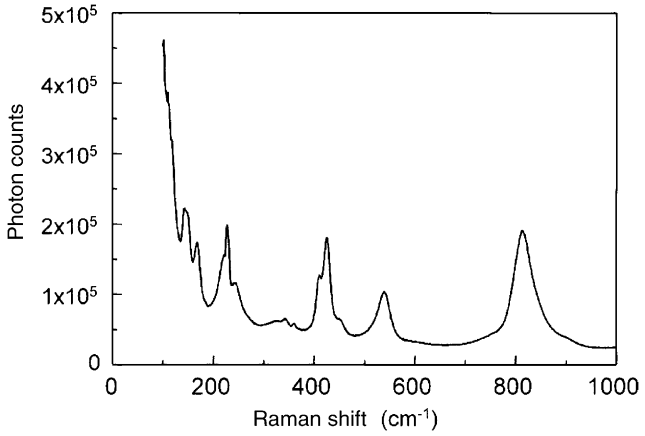

Fig. 6. Shows the room temperature Raman spectrum of the equilibrium Sr_2InNbO_6 compound (cf. with Fig. 4 of Ref. [11]).

equilibrium $Sr(In_{0.5}Nb_{0.5})O_3$ compound (see Fig. 6) is much more like the Raman spectra reported for other $Sr(B_{0.5}Nb_{0.5})O_3$ compounds in Ref. [11] and nothing like that reported in the same paper for $Sr(In_{0.5}Nb_{0.5})O_3$.

3.3. Local crystal chemical considerations

The highest possible space group symmetry compatible with rock salt type B cation ordering of an A_2InNbO_6 double perovskite is $Fm\bar{3}m$, $a = 2a_p$ [5,6] with In at 000, Nb at $0\,0\,\frac{1}{2}$, A at $\frac{1}{4},\frac{1}{4},\frac{1}{4}$ and O at $(\frac{1}{4}+\varepsilon_1)\,0\,0$ (see Fig. 1). Note that there are only two structural degrees of freedom, the overall lattice parameter $a = 2a_p$ and the parameter ε_1 describing the crystal chemically necessary expansion in size of the InO_6 octahedra and associated contraction of the NbO_6 octahedra.

Given that there are four ions (A^{2+}, In^{3+}, Nb^{5+} and O^{2-}) whose local crystal chemical requirements all need to be satisfied, it would not be surprising if the two $Fm\bar{3}m$ symmetry-allowed structural degrees of freedom were insufficient to simultaneously satisfy the competing bond valence requirements of all these ions. This can be shown nicely via a plot of the percentage deviation in calculated bond valence sum (or apparent valence, AV) away from the ideal AV [16], Δ(AV)/AV, for each of the constituent cations as a function of ε_1 for each of the A = Ba, Sr and Ca compounds (see Fig. 7). In the case of the A = Ca compound, where the metric symmetry is no longer cubic, we have used an average a of 2×3.9707 Å (obtained from the refined metrically orthorhombic cell dimensions obtained earlier) for the purposes of this bond valence sum calculation.

In each case, it can be seen that the In^{3+} ions (corresponding to the open circles in Fig. 7) would be very significantly over-bonded and the Nb^{5+} ions (corresponding to the triangles in Fig. 7) very significantly under-bonded without an expansion in size of the

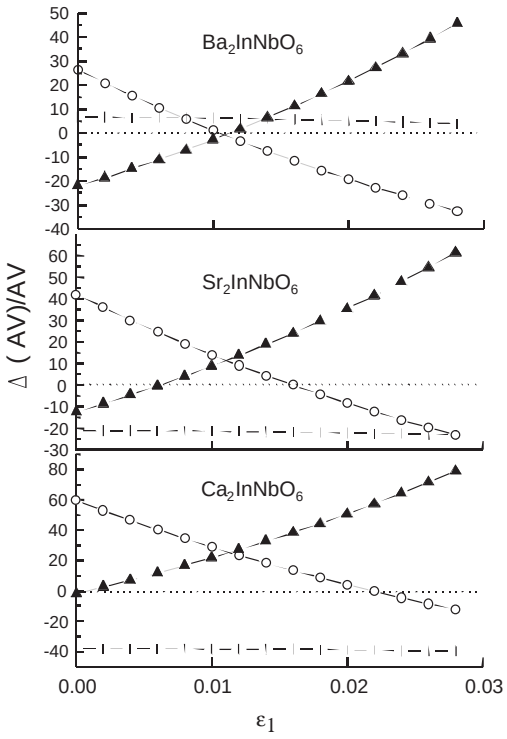

Fig. 7. Shows a plot of Δ(AV)/AV, for each of the constituent cations as a function of ε_1 for each of the A = Ba, Sr and Ca compounds assuming $Fm\bar{3}m$, $a = 2a_p$ resultant space group symmetry. The In^{3+} ions are represented by the line drawn through the open circles, the Nb^{5+} ions by the line drawn through the filled triangles and the A^{2+} ions by the line drawn through the vertical dashes. The ideal Δ(AV)/AV = 0 line is drawn as a dashed horizontal in each case.

InO_6 octahedra and a contraction in size of the NbO_6 octahedra, i.e. at $\varepsilon_1 = 0$. As ε_1 increases, the InO_6 octahedra expand while the NbO_6 octahedra contract. The initial over-bonding of the In ions thus reduces as does the under-bonding of the Nb ions until the two Δ(AV)/AV curves intersect at $\varepsilon_1 \sim 0.0113$ ($\equiv \sim 0.09$ Å shift of the O ion position from its ideal perovskite parent position) in each case. For the A = Ba compound, both the In and Nb ions are essentially happily bonded at this intersection point while the Ba ion is, if anything slightly over-bonded ($\sim 6.5\%$). There is thus no need for additional octahedral rotation in the case of the A = Ba compound (indeed the Ba ions would resist any such octahedral rotation) and one should therefore expect, as has been found experimentally, the resultant space group symmetry for this compound to be $Fm\bar{3}m$.

For the A = Sr and Ca compounds, however, the In^{3+} and Nb^{5+} ions are both significantly over-bonded (by $\sim 11\%$ for the A = Sr compound and by $\sim 25\%$ for the A = Ca compound) while the interstitial A ion is significantly under-bonded (by $\sim 21\%$ for the A = Sr compound and $\sim 38\%$ in the case of the A = Ca compound) at the equivalent intersection point, i.e. additional octahedral rotation expanding the size of the

local InO_6 and NbO_6 octahedra (thereby reducing the over-bonding of the In and Nb ions) while simultaneously collapsing the anion co-ordination polyhedra around the interstitial A cation (thereby reducing the under-bonding of the interstitial A cations) is clearly essential in order to satisfy local bond valence requirements in the case of the A = Sr and Ca compounds.

Re-setting the $Fm\bar{3}m$, $a = 2a_p$ fractional co-ordinates given above into the resultant $P12_1/n1$, $\mathbf{a} = \mathbf{a}_p + \mathbf{b}_p$, $\mathbf{b} = -\mathbf{a}_p + \mathbf{b}_p$, $\mathbf{c} = 2\mathbf{c}_p$, setting gives the following fractional co-ordinates: In at 0 0 0; Nb at $0\,0\,\frac{1}{2}$; A at $\frac{1}{2}, 0, \frac{1}{4}$; O1 at $(\frac{1}{4}+\varepsilon_1)$, $-(\frac{1}{4}+\varepsilon_1)$, 0; O2 at $(\frac{1}{4}+\varepsilon_1)$, $(\frac{1}{4}+\varepsilon_1)$, 0 and O3 at $0,0,(\frac{1}{4}+\varepsilon_1)$, respectively. We now need to include the effect of additional octahedral rotation around both the resultant **b**- and **c**-axis as implied by Fig. 7 and the resultant $P12_1/n1$ space group symmetry [6]. Such octahedral rotation does not affect the positions of the cations just given but does alter the fractional co-ordinates of the three independent O ions per resultant supercell to $(\frac{1}{4}+\varepsilon_1+\varepsilon_2)$, $(-\frac{1}{4}-\varepsilon_1+\varepsilon_2)$, $(0-\varepsilon_3)$ for O1; to $(\frac{1}{4}+\varepsilon_1-\varepsilon_2)$, $(\frac{1}{4}+\varepsilon_1+\varepsilon_2)$, $(0-\varepsilon_3)$ for O2 and to to $(0+2\varepsilon_3)$, 0, $(\frac{1}{4}+\varepsilon_1)$ for O3. In this notation, the parameter ε_1 ($\sim$0.0113) represents coupled expansion/contraction of the InO_6/NbO_6 octahedra, ε_2 represents octahedral rotation around **c** while ε_3 represents octahedral rotation around **b**. Furthermore, in order to maintain octahedral regularity (i.e. in order for the distance from In to O1 and O2 to be the same as the distance from In to O3, etc.), at least in the small amplitude regime, it is necessary for $|\varepsilon_2| = |\varepsilon_3| = \varepsilon_{2,3}$. We have thus assumed that $\varepsilon_2 = \varepsilon_3 = \varepsilon_{2,3}$. Adding this additional constraint gives the final O ion fractional co–ordinates as $(\frac{1}{4}+\varepsilon_1+\varepsilon_{2,3})$, $(-\frac{1}{4}-\varepsilon_1+\varepsilon_{2,3})$, $(0-\varepsilon_{2,3})$ for O1; $(\frac{1}{4}+\varepsilon_1-\varepsilon_{2,3})$, $(\frac{1}{4}+\varepsilon_1+\varepsilon_{2,3})$, $(0-\varepsilon_{2,3})$ for O2 and $(0+2\varepsilon_{2,3})$, 0, $(\frac{1}{4}+\varepsilon_1)$ for O3. Given that Fig. 5 enables us to fix ε_1 at $\sim$0.0113, the only remaining degree of freedom is the rotational amplitude parameter $\varepsilon_{2,3}$.

Fig. 8 shows a plot of Δ(AV)/AV for each of the constituent cations as a function of $\varepsilon_{2,3}$ for both the A = Sr and Ca compounds. Note that we have again assumed cubic metric symmetry in calculating the AVs. This is obviously an approximation. In both cases, it can be seen that the In^{3+} and Nb^{5+} ions are significantly over-bonded and the A^{2+} ions significantly under-bonded without octahedral rotation, i.e. at $\varepsilon_{2,3} = 0$. As $\varepsilon_{2,3}$ increases, the InO_6 and NbO_6 octahedra simultaneously expand while the A^{2+} co-ordination polyhedra contracts. The initial over-bonding of the In^{3+} and Nb^{5+} ions thus systematically reduces as does the under-bonding of the A^{2+} ions until each of the Δ(AV)/AV curves cross the ideal zero position almost simultaneously at $\varepsilon_{2,3} \sim 0.0352$ ($\equiv$an octahedral rotation around **c** of $\theta_z \sim 7.95°$ and around **b** of $\theta_y \sim 7.95\sqrt{2} = 11.24°$) in the case of the A = Sr compound and at $\varepsilon_{2,3} \sim 0.052$ ($\equiv$an octahedral rotation around **c** of $\theta_z \sim 11.7°$ and around **b** of $\theta_y \sim 11.7\sqrt{2} = 16.5°$) in the case of the A = Ca compound. At this point, all ions are essentially happily bonded in both cases (see Table 1). The predicted ($\varepsilon_1 = 0.0113$, $\varepsilon_{2,3} = 0.0352$) Sr_2InNbO_6 compound is shown in projection down the (a) $\langle 001 \rangle$ and (b) $\langle 010 \rangle$ directions in Fig. 9.

Substitution of these bond valence sum determined values for ε_1 and $\varepsilon_{2,3}$ into the expressions given above for the O ion fractional co-ordinates (see Table 1) should thus lead to a pretty good zeroth order approximation to the resultant structures of both the A = Sr and Ca compounds. These predicted fractional co-ordinates

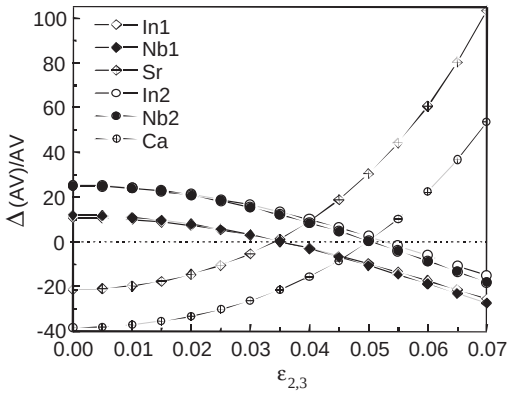

Fig. 8. Shows a plot of Δ(AV)/AV for each of the constituent cations as a function of the rotational amplitude parameter $\varepsilon_{2,3}$ for both the A = Sr and Ca compounds assuming resultant $P12_1/n1$ ($\mathbf{a} = \mathbf{a}_p + \mathbf{b}_p$, $\mathbf{b} = -\mathbf{a}_p + \mathbf{b}_p$, $\mathbf{c} = 2\mathbf{c}_p$) resultant space group symmetry. The In and Nb ions associated with the A = Sr compound are labelled In1 and Nb1 while the In and Nb ions associated with the A = Ca compound are labelled In2 and Nb2.

Table 1
Predicted resultant fractional co-ordinates for Sr_2InNbO_6 (first row) and Ca_2InNbO_6 (second row)

Atom label	x	y	z	AV[a]
A-ion (Sr)	1/2	0	1/4	2.030
(Ca)	1/2	0	1/4	2.047
In	0	0	0	3.001
	0	0	0	3.030
Nb	0	0	1/2	4.999
	0	0	1/2	4.945
O(1)	0.2965	0.7739	0.9648	2.010
	0.3133	0.7907	0.9480	1.981
O(2)	0.2261	0.2964	0.9648	2.010
	0.2093	0.3133	0.9480	2.008
O(3)	0.0704	0	0.2613	2.010
	0.1040	0	0.2613	2.046

[a] $P12_1/n1$, $a = 5.7375$, $b = 5.7375$, $c = 8.1140$ Å, $\beta = 90°$ in the case of the A = Sr compound. $P12_1/n1$, $a = 5.5284$, $b = 5.7109$, $c = 7.9290$ Å, $\beta = 90°$ in the case of the A = Ca compound.

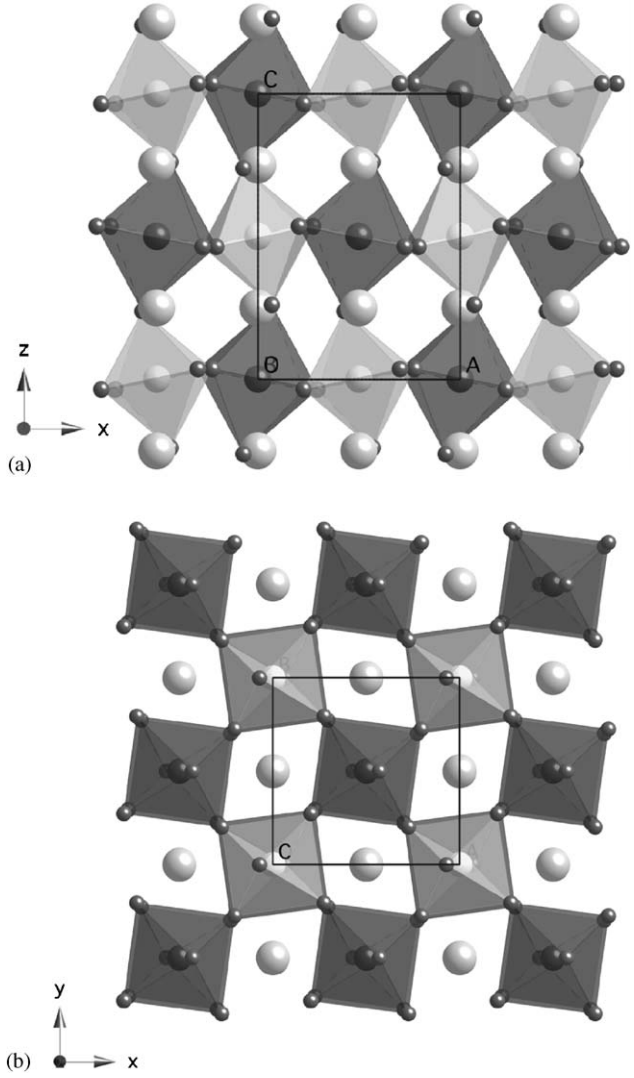

Fig. 9. Shows the predicted ($\varepsilon_1 = 0.0113$, $\varepsilon_{2,3} = 0.0352$) Sr_2InNbO_6 compound in projection down the (a) $\langle 010 \rangle$ and (b) $\langle 001 \rangle$ directions. The larger InO_6 octahedra are represented by the darker octahedra while the lighter octahedra represent the smaller NbO_6 octahedra. The Sr ions are presented by the largest gray balls and the O ions by the smallest darker balls.

cannot, however, be expected to be perfect as a result of the approximations inherent in the above bond valence sum analysis—in particular, we have ignored the orthorhombic metric symmetry of the $A = Ca$ compound and also used a small rotation amplitude approximation which is clearly not strictly valid, particularly in the case of the $A = Ca$ compound. Rietveld refinement of high-quality diffraction data (preferably neutron diffraction data in order to enhance the refineability of the O ion positions) is thus still needed in order to precisely refine the $P12_1/n1$ crystal structures of these $A = Sr$ and Ca double perovskite compounds.

References

[1] A.M. Glazer, Acta Crystallogr. B 28 (1972) 3384–3392.
[2] H.D. Megaw, Crystal Structures—A Working Approach, W.B. Saunders, Philadelphia, 1973.
[3] C.J. Howard, H.T. Stokes, Acta Crystallogr. B 54 (1998) 782–789.
[4] C.J. Howard, R.L. Withers, B.J. Kennedy, J. Solid State Chem. 160 (2001) 8–12.
[5] M.T. Anderson, K.B. Greenwood, G.A. Taylor, K.R. Poeppelmeier, Prog. Solid State Chem. 22 (1993) 197–233.
[6] C.J. Howard, B.J. Kennedy, P.M. Woodward, Acta Crystallogr. B 59 (2003) 463–471.
[7] I. Levin, J.Y. Chan, R.G. Geyer, J.E. Maslar, T.A. Vanderah, J. Solid State Chem. 156 (2001) 122–134.
[8] C. Chou, D. Tsai, I. Lin, J.W. Steeds, Mater. Chem. Phys. 79 (2003) 218–221.
[9] I. Qazi, I.M. Reaney, W.E. Lee, J. Eur. Ceramic Soc. 21 (2001) 2613–2616.
[10] J. Yin, Z. Zou, J. Ye, J. Phys. Chem. B 107 (2003) 61–65.
[11] R. Ratheesh, M. Wöhlecke, B. Berge, Th. Wahlbrink, H. Haeuseler, E. Rühl, R. Blachnik, P. Balan, N. Santha, M.T. Sebastian, J. Appl. Phys. 88 (2000) 2813–2818.
[12] F. Galasso, W. Darby, J. Phys. Chem. 66 (1962) 131–132.
[13] V.S. Filip'ev, E.G. Fesenko, Sov. Phys.—Crystallogr. 10 (1966) 532–534.
[14] V.S. Filip'ev, E.G. Fesenko, Sov. Phys.—Crystallogr. 10 (1966) 243–247.
[15] A.J.C. Wilson (Ed.), International Tables for Crystallography, Vol. A, Kluwer Academic Publishers, Dordrecht, 1995.
[16] N.E. Brese, M. O'Keeffe, Acta Crystallogr. B 47 (1991) 192–198.